Neurobiology of Aging 68 (2018) 114–122

Contents lists available at ScienceDirect

Neurobiology of Aging

journal homepage: www.elsevier.com/locate/neuaging

Longitudinal accrual of neocortical amyloid burden is associated with microstructural changes of the fornix in cognitively normal adults

Zhuang Song [a,*], Michelle E. Farrell [a], Xi Chen [a], Denise C. Park [a,b]

[a] Center for Vital Longevity, University of Texas at Dallas, Dallas, TX, USA
[b] Department of Psychiatry, University of Texas Southwestern Medical Center, Dallas, TX, USA

ARTICLE INFO

Article history:
Received 20 September 2017
Received in revised form 20 February 2018
Accepted 21 February 2018
Available online 6 March 2018

Keywords:
Fornix
Hippocampus
Amyloid
Alzheimer's disease
Diffusion tensor imaging

ABSTRACT

The fornix and parahippocampal cingulum are 2 major limbic tracts in the core memory network of the hippocampus. Although these fiber tracts are known to degrade with Alzheimer's disease (AD), little is known about their vulnerability in the asymptomatic phase of AD. In this longitudinal study of cognitively normal adults, we assessed amyloid-beta (Aβ) plaques using positron emission tomography and white matter microstructure using diffusion tensor imaging. We found that an increase of neocortical Aβ burden over time was associated with an increase of radial diffusivity in the fornix but not in the parahippocampal cingulum. The effect of increasing neocortical Aβ burden on the fornix remained significant after controlling for baseline measures, head motion, global brain atrophy, regional Aβ burden in the hippocampus, or microstructural changes in the global white matter. In addition, microstructural changes in the fornix were not associated with decline of episodic memory or other cognitive abilities. Our findings suggest that microstructural changes in the fornix may be an early sign in the asymptomatic phase of AD.

1. Introduction

Alzheimer's disease (AD) is a common type of dementia that is characterized by deposition of amyloid-beta (Aβ) plaques and tau tangles in brain networks (Selkoe, 2002). Memory loss is a prominent clinical symptom of AD. There is mounting evidence that core memory structures in the medial temporal lobe (MTL), including the hippocampus and parahippocampal gyrus, are particularly vulnerable to AD (Braak and Braak, 1991; Small et al., 2011). Neurodegeneration in the MTL has been long thought to be essentially responsible for memory decline in the course of AD (Gallagher and Koh, 2011; Jack et al., 1997; Petersen et al., 2000; Sperling et al., 2010).

The fornix and parahippocampal cingulum (PHC-cingulum) are 2 prominent limbic white matter tracts that connect the MTL structures to other memory-related brain structures. Specifically, the fornix is a bidirectional fiber tract that contains both afferent and efferent pathways connecting the hippocampus with a number of subcortical and cortical structures; the PHC-cingulum tract contains predominately afferent fibers to the MTL, but not directly to the hippocampus, from the cingulate cortex and other cortical structures (Aggleton, 2014; Catani et al., 2013; Mori and Aggarwal, 2014; Mufson and Pandya, 1984). There is increasing evidence that synaptic dysfunction and axonal degeneration may long precede somatic cell death in the course of AD (Ittner and Gotz, 2011; Jin et al., 2011; Kanaan et al., 2013; Menkes-Caspi et al., 2015; Selkoe, 2002), suggesting that white matter degradation may precede brain volume loss. Degradation of fiber integrity in both the fornix and PHC-cingulum is observed in AD patients (Kantarci et al., 2017; Nir et al., 2013; Solodkin et al., 2013), but little is known about the vulnerability of these fiber tracts in the earliest phase of AD. In the decades-long period of asymptomatic development of AD, neocortical Aβ deposition is elevated in cognitively normal older adults (Hardy and Selkoe, 2002; Jack and Holtzman, 2013; Jack et al., 2010) and is recognized as a major biomarker of preclinical AD (Sperling et al., 2011). The focus of the present study is to assess potential changes in the limbic white matter tracts at the preclinical stage of AD characterized by neocortical Aβ burden in cognitively normal adults.

The advent of diffusion tensor imaging (DTI) has permitted examination of microstructures of white matter tracts, relying on water diffusivity as an indirect measurement of fiber integrity (Basser and Pierpaoli, 1996). Several cross-sectional studies of DTI have examined the relationship of Aβ deposition to microstructures of the fornix and PHC-cingulum in cognitively normal older adults (Chao et al., 2013; Gold et al., 2014; Racine et al., 2014), although results

* Corresponding author at: Center for Vital Longevity, University of Texas at Dallas, 1600 Viceroy Drive, Suite 800, Dallas, TX 75235, USA. Tel.: +1 972 883 3718; fax: +1 972 883 3250.
E-mail address: zhuang.song@utdallas.edu (Z. Song).

https://doi.org/10.1016/j.neurobiolaging.2018.02.021

have been inconsistent. For instance, 2 studies found that higher Aβ burden in the brain was related to lower fractional anisotropy (FA) in the fornix (Chao et al., 2013; Gold et al., 2014), whereas another reported the opposite (Racine et al., 2014). Similarly, cross-sectional DTI studies of autosomal-dominant AD mutations carriers in the preclinical stage have also generated mixed findings. For instance, 1 study found the effect of presymptomatic mutations on microstructure in the fornix (Ringman et al., 2007), whereas another study failed to find such an effect (Sanchez-Valle et al., 2016). In comparison with cross-sectional studies, a longitudinal design directly assesses changes within each individual. A recent longitudinal study of cognitively normal adults found that higher neocortical Aβ burden at the baseline predicted a faster reduction of FA in PHC-cingulum in approximately 3 years, but the fornix was not examined (Rieckmann et al., 2016). Given the importance of both the fornix and PHC-cingulum in the core memory network, it is of great interest to assess both tracts within the same study sample.

The focus of the present longitudinal study is to determine whether increasing neocortical Aβ burden is related to microstructural changes in the fornix or PHC-cingulum in cognitively normal adults. An affirmative relationship would suggest that degradation in these fiber tracts may be an early signal of AD. We examined the longitudinal relationship between neocortical Aβ burden and white matter microstructure of both the fornix and PHC-cingulum in cognitively normal adults aged 55–89 years, over an approximately 4-year interval, using positron emission tomography (PET) of Aβ in conjunction with DTI. We first examined the cross-sectional relationship of neocortical Aβ burden to microstructural assessments in the fornix and PHC-cingulum at both the baseline and follow-up. Then, in the primary analysis, we related annual change of neocortical Aβ burden to annual changes of DTI indices in both fiber tracts. Finally, we examined whether microstructure changes in the fornix or PHC-cingulum, which are important fiber tracts in the core memory network, were predictive of changes in episodic memory and other cognitive variables.

2. Materials and methods

2.1. Participants

The sample initially consisted of 55 cognitively normal adults (aged 55–89 years at baseline) drawn from the Dallas Lifespan Brain Study (DLBS) who had PET and DTI scans at both the baseline and follow-up. Three participants were excluded either for corrupted DTI data or for poor image registration. The final study sample consisted of 52 participants. All participants were right-handed, with English as their primary language, did not have major heart and neurological diseases, and had a Mini–Mental State Examination (MMSE) score of 26 or greater at baseline (mean = 28.0 ± 1.2) and 25 or greater at follow-up (mean = 29.0 ± 1.2). Participants completed the same protocols at baseline and approximately 4 years later. One participant missed all the cognitive tests at both the baseline and follow-up. Two other participants missed tests for episodic memory at the follow-up. Informed consent for the study was collected in accordance with the policy of the Institutional Review Board of the University of Texas Southwestern Medical Center and the University of Texas at Dallas. Demographic information for the participants is presented in Table 1. Thirteen participants had at least 1 APOE-e4 allele (25%).

2.2. Magnetic resonance imaging acquisition

Magnetic resonance imaging data were acquired in a Philips Achieva 3-Tesla scanner (Philips Medical Systems, Best, The Netherlands) equipped with an 8-channel head coil. T1-weighted 3-dimensional high-resolution anatomical images were acquired with magnetization-prepared rapid gradient-echo pulse sequence (field of view = 256 × 256 mm^2, matrix size = 256 × 256, repetition time = 8.18 ms, echo time = 3.76 ms, flip angle = 12°, voxel size 1 × 1 × 1 mm^3, and 160 sagittal slices). Diffusion-weighted images (DWIs) were acquired with whole-brain T2*-weighted interleaved echo-planar images (sensitivity encoding = 2, field of view = 224 × 224 mm^2, matrix size = 128 × 128, repetition time = 4410 ms, echo time = 51 ms, flip angle = 90°, 50 axial slices of 2 mm thickness with 1 mm slice gap, b = 1000 s/mm^2 with 30 directions, and one b = 0 frame). Raw images from the scanner were converted to Neuroimaging Informatics Technology Initiative format using r2agui.

Table 1
Demographic characteristics and cognitive performance at both time points of assessments

	Time 1	Time 2
N	52	
Gender (female/male)	38/14	
Education range (years)	12 to ~21	
Education (years)	15.9 (2.6)	
ApoE4 allele (N)	13	
Testing interval of MRI (years)	4.0 (0.2)	
Testing interval of PET (years)	3.4 (0.2)	
Age range at baseline	54.7 to ~89.1	58.7 to ~93.1
Age at baseline	70.7 (9.2)	74.7 (9.1)
Body mass index	26.3 (3.2)	26.1 (3.3)
MMSE range	26 to ~30	25 to ~30
MMSE	28.0 (1.2)	29.0 (1.2)
Episodic memory (z-score)	0.013 (0.770)	0.070 (0.769)
Processing speed (z-score)	0.315 (0.820)	−0.231 (0.940)*
Fluid reasoning (z-score)	−0.030 (0.821)	0.044 (0.806)
Crystallized intelligence (z-score)	0.051 (0.938)	−0.073 (1.000)
Neocortical SUVr	0.775 (0.133)	0.807 (0.156)***

Note: Mean and standard deviations (in parenthesis) are reported for continuous variables. The asterisk symbols indicate significance levels of paired 2-sided *t*-tests across time points: *, $p<0.05$ and ***, $p<0.001$.
Key: Aβ, amyloid-beta; MMSE, Mini–Mental State Examination; MRI, magnetic resonance imaging; N, number of participants; SUVr, standard uptake value ratio; PET, positron emission tomography.

2.3. PET acquisition and processing

The PET scan was performed on the Siemens ECAT HR PET scanner. Participants were injected with a 370-MBq (10 mCi) bolus of F18-AV-45 florbetapir radiotracer. At 30 minutes after injection, participants were positioned on the imaging table of the scanner. Soft Velcro straps and foam wedges were used to secure the participant's head, which was positioned with laser guides. A 2-frame, by 5 minutes each, dynamic emission was acquired 50 minutes after the injection of the florbetapir radiotracer, immediately after a 7-minute scan of internal rod source transmission. The transmission images were reconstructed using back-projection and a 6-mm full width at half maximum gaussian filter. To limit noise associated with using multiple time points and to avoid bias to either time point, each MPRAGE and their associated PET scans were coregistered to the mean MPRAGE image of each participant (created using FreeSurfer v5.3). A single set of regions of interest (ROIs) was created for each subject by taking the conjunction of the FreeSurfer parcellations from each time point. Standardized uptake value ratio (SUVr) in the neocortex was defined as the ratio of mean Aβ tracer uptake in 7 predefined neocortical gray matter regions (dorsal lateral prefrontal cortex, orbitofrontal cortex, lateral parietal cortex, isthmus cingulate cortex, rostral anterior cingulate cortex, precuneus, and lateral temporal cortex) normalized to the mean of a reference region including the cerebellum and subcortical white matter. Using this reference region for the consideration of longitudinal data stability in PET, however, results in a lower range of values for SUVr, with SUVr < 1 even with substantial Aβ load in the brain (Landau et al., 2015; Schwarz et al., 2017).

It remains an active research topic on how to define a clinically meaningful threshold of SUVr in cognitively normal adults (Mormino et al., 2012; Villeneuve et al., 2015). Using different thresholds based on SUVr may lead to different findings (Farrell et al., 2017). Therefore, the present study was focused on treating the status of neocortical Aβ load as a continuous variable.

2.4. Behavioral measures

The cognitive battery, completed by all participants at both time points, was used to create scores in 4 cognitive domains. In each cognitive domain, z-scores were created for individual indictors across all participants at both time points and then were averaged to create a composite score. The main composite of interest was episodic memory, with 4 indicators: (1) the number of correct items on immediate free recall; (2) the number of correct items on delayed free recall; (3) accuracy in delayed recognition of the Hopkins Verbal Leaning Task (Brandt, 1991); and (4) the number of correct items free recalled on the Verbal Recognition Memory task from the Cambridge Neuropsychological Test Automated Battery (Robbins et al., 1994), Cronbach α = 0.838. The processing speed composite included the number of correct items on the Digit Symbol task (Wechsler, 1997) and the Digit Comparison task (Salthouse and Babcock, 1991), Cronbach α = 0.801. The fluid reasoning composite had 3 indicators: (1) the total score on the Educational Testing Service Letter Sets task (Ekstrom et al., 1976); (2) the number of correct items on the Raven's Progressive Matrices task (Raven et al., 1998); and (3) the number of problems solved in the minimum number of moves required on the Stockings of Cambridge task from the Cambridge Neuropsychological Test Automated Battery (Robbins et al., 1994), Cronbach α = 0.704. Crystallized intelligence was measured using a single task based on the total number of correct items on the Educational Testing Service Advanced Vocabulary Scale (Ekstrom et al., 1976).

2.5. DTI processing

DWIs were processed and analyzed using the FSL software suite (Jenkinson et al., 2012). All DWI frames were coregistered with the b = 0 frame with affine registration to partially correct for image distortion induced by eddy current in addition to head motion. Skull stripping was first done in the b = 0 frame for the best tissue contrast, and then the resulted mask was applied to all DWI frames. A diffusion tensor model was constructed at each voxel. Radial diffusivity (RD), axial diffusivity (AXD), mean diffusivity (MD), and FA were derived from the tensor model (Basser and Pierpaoli, 1996). The diffusivity unit is mm^2/s.

We assessed head motion across DWI frames during the acquisition. Head motion of each DWI frame was assessed relative to the b = 0 reference frame, based on the affine registration parameters, with a total motion index (TMI) that was previously described (Yendiki et al., 2013). Specifically, the TMI was computed as average displacement of all the 30 DWI frames to the b = 0 frame, which included the translation and rotation of each frame. Furthermore, we used 2 metrics to account for the TMI at both baseline and follow-up: (1) the mean TMI at both time points and (2) the difference of TMI between the 2 time points.

2.6. Template construction for DTI

For group analyses, we constructed a sample-specific DTI-FA template using the Advanced Normalization Tools (ANTS) (Avants and Gee, 2004; Avants et al., 2014), which was validated in FA image registration in white matter tracts that included the fornix and cingulum (Schwarz et al., 2014). The spatial registration of each individual FA volume to the FA template was established with the template construction. Individual RD and AXD volumes were then registered to the FA template based on the same registration of the corresponding FA volume. Anatomical ROIs of the bilateral fornix and PHC-cingulum were identified in the Johns Hopkins University (JHU) ICBM-DTI-81 FA template (Mori et al., 2008). It is noted that

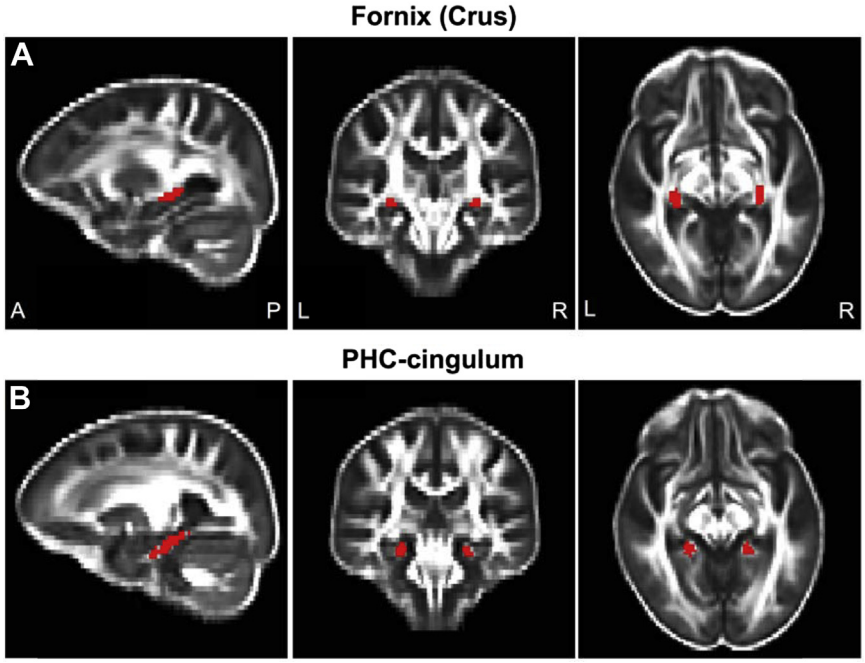

Fig. 1. Bilateral anatomical regions of interest of the fornix crus (A) and PHC-cingulum (B) in the sample-specific fractional anisotropy template. The region of interest is indicated by red color in each row, where three views are displayed from left to right: saggital, coronal, and axial. Abbreviations: A, anterior; L, left; P, posterior; PHC-cingulum, parahippocampal cingulum; R, right. (For interpretation of the references to color in this figure legend, the reader is referred to the Web version of this article.)

the fornix was not separated in this template from the stria terminalis, another small fiber tract connecting to the amygdala in the limbic system (Mori et al., 2008). These ROIs were registered to the sample-specific FA template via the JHU FA template by ANTS (Fig. 1). In addition, we excluded voxels within each ROI if the mean FA values were lower than 0.2 so that the white matter ROI masks were approximately located within the white matter in each individual image. After this processing, the size of the bilateral fornix ROI was 1791.6 mm^3 (195 voxels) and the size of the bilateral PHC-cingulum ROI was 2021.3 mm^3 (220 voxels) in the sample-specific FA template. The size of the global white matter ROI of the brain was 140,311.5 mm^3 (15,272 voxels) in which the fornix and PHC-cingulum were excluded. It is important to note that the fornix ROI was limited to the crus for the following reasons. First, the crus was better identified than other parts of the fornix in the JHU ICBM-DTI-81 template likely because that the crus has a more uniform arrangement of fibers and less branching connections than the body and columns (Malykhin et al., 2008). Second, because the crus is the most adjacent part of the fornix to the hippocampus, it is likely to be more vulnerable than other parts of the fornix to the pathology spreading from the hippocampus and other MTL structures (Kantarci et al., 2017). Third, the ROI size of the body and column was only about one-third of the crus of the fornix in the JHU template. A smaller ROI is more prone to errors in spatial alignments across participants. In addition to the problem of cerebrospinal fluid (CSF) contamination in DTI, measurement in the body and column would be therefore much less reliable than the crus of the fornix. Nevertheless, we describe the analyses of the body and column of the fornix in Supplementary Materials.

2.7. Statistical analysis

We first used cross-sectional data to assess whether neocortical Aβ burden (i.e., SUVr) had any effects on microstructural measures of the fornix crus or PHC-cingulum. Then, in the primary general linear regression analyses, we used longitudinal data to assess whether changes in neocortical SUVr tracked with changes in the DTI indices of the same fiber tracts, with age and gender controlled. Next, we conducted a series of secondary analyses where we added 1 additional variable each time to the original model, allowing us to determine if the primary effect remained significant after taking into account each additional variable. These analyses are summarized in Table 2 that shows 4 categories of variables: (1) mean and difference of head motion (i.e., TMI) during DTI acquisition at baseline and follow-up; (2) baseline and annual change rate of global brain atrophy, which was measured as total cortical volume (TCV) normalized by intracranial volume using the FreeSurfer segmentation; (3) baseline and annual change rate of regional SUVr in the hippocampus based on the anatomical mask from the FreeSurfer parcellation; and (4) baseline and annual change rate of both MD and FA of the global white matter that excluded the fornix and PHC-cingulum. These 4 types of variables were considered for different reasons. First, head motion may introduce imaging artifacts in DTI (Yendiki et al., 2013). Second, age-related brain atrophy may contaminate DTI assessments of the white matter for partial volume effects with increased extracellular water (Madden et al., 2012). Third, from a pathogenesis perspective, regional Aβ burden in the hippocampus may have different impacts on closely connected limbic tracts in comparison with global Aβ burden. Although the MTL structures have generally low susceptibility to neuritic Aβ plaques (Braak and Braak, 1991; Grothe et al., 2017), we nevertheless considered that Aβ plaques might be present in the hippocampus in some participants, and that increases of Aβ deposition in the hippocampus over time could be more directly related to microstructural changes in the fornix. It is noted that analyses of the regional SUVr in the hippocampus were independent from the primary analysis of the composite neocortical SUVr, as the 7 regions used to develop the composite were all outside of the MTL. Fourth, DTI measures of the global white matter were taken into account to assess how much local changes in the limbic tracts reflected global changes in the white matter. Each of the additional variables was analyzed separately for conceptual clarity and to preserve power because of the limited sample size in the present study.

Finally, we examined relationships between DTI indices and cognition. We first used cross-sectional data to relate the DTI indices to episodic memory and to other cognitive variables. We then used longitudinal data to examine whether annual changes in the DTI indices were related to annual changes in episodic memory or to other cognitive variables.

Table 2
Summary of the secondary statistical analyses

	R^2	p value	R^2 changed from original model	Proportion R^2 changed from original model
Original model	0.158	0.003	–	–
Modified model with additional variable being controlled				
Head motion (TMI)				
Mean of baseline and follow-up	0.169	0.002	0.011	0.070
Baseline to follow-up	0.157	0.004	−0.001	−0.006
Normalized total cortical volume				
Baseline	0.156	0.004	−0.002	−0.013
Annual change rate	0.100	0.022	−0.058	−0.367
Hippocampal Aβ burden (SUVr)				
Baseline	0.150	0.005	−0.008	−0.051
Annual change rate	0.126	0.010	−0.032	−0.203
Global white matter microstructure				
Baseline MD	0.103	0.021	−0.055	−0.348
Annual change rate of MD	0.070	0.058	−0.088	−0.557
Baseline FA	0.158	0.004	0.000	0.000
Annual change rate of FA	0.141	0.006	−0.017	−0.108

The original model assessed the primary effect of annual change rate of neocortical SUVr on annual change rate of RD in the fornix crus, for which age and gender were controlled. In each modified model, an additional variable was controlled. The coefficient R^2 and significance level p value were reported for the primary effect. In addition, relative to the original model, change and proportion change of R^2 in each modified model were reported.
Key: Aβ, amyloid-beta; FA, fractional anisotropy; MD, mean diffusivity; RD, radial diffusivity; SUVr, standard uptake value ratio; TMI, total motion index during diffusion tensor imaging acquisition.

3. Results

3.1. Relationship of neocortical Aβ burden to microstructures of the limbic tracts in cross-sectional data

We first conducted general linear analyses at baseline that assessed the relationships between neocortical Aβ burden and the 3 primary DTI indices (AXD, RD, and FA), respectively, for both tracts in the fornix crus and PHC-cingulum, with age and gender controlled. We found that higher neocortical SUVr was marginally related to higher RD ($R^2 = 0.07$, $p = 0.06$), but not significantly to AXD ($R^2 = 0.04$, $p = 0.16$) or FA ($R^2 = 0.04$, $p = 0.14$), in the fornix crus. There were no significant effects of neocortical SUVr on any DTI indices in the PHC-cingulum ($R^2 < 0.001$, $p > 0.80$).

We also assessed these cross-sectional relationships for the follow-up data collected approximately 4 years later. With age and gender controlled, higher neocortical SUVr was related to higher RD ($R^2 = 0.12$, $p = 0.01$), and marginally related to AXD ($R^2 = 0.07$, $p = 0.06$) and FA ($R^2 = 0.05$, $p = 0.12$), in the fornix crus. There were no significant effects of neocortical SUVr on any DTI indices in the PHC-cingulum ($R^2 < 0.001$, $p > 0.80$). After multiple comparison correction with the false discovery rate (FDR) method among the 6 tests (3 DTI indices × 2 ROIs), the effect of neocortical SUVr approached significance on RD ($p = 0.06$), but not on the AD or FA ($p > 0.20$), in the fornix crus.

In summary, we found limited evidence that higher neocortical SUVr was related to RD of the fornix crus at follow-up but not at baseline.

3.2. Annual changes in cortical Aβ deposition and microstructures of the limbic tracts

In this set of analyses, we assessed longitudinal changes in neocortical Aβ burden and DTI measures of microstructures in the tracts of interest. Fig. 2 shows the spaghetti plot of neocortical SUVr measured at baseline and follow-up. A 1-sample *t*-test showed that the annual change rate of neocortical SUVr was above zero ($t = 5.39$, $p < 0.0001$). A multiple linear regression analysis found that greater annual change of neocortical SUVr was related to higher neocortical SUVr at baseline ($p = 0.01$) but not related to APOE-e4 status, age, or gender ($p > 0.20$).

For the DTI indices, 1-sample t-tests showed that the annual change rates of RD and AXD was above zero and the annual change rate of FA was below zero in the bilateral ROIs of the fornix crus and PHC-cingulum, respectively ($|t| > 2.34$, $p < 0.05$). Among all these changes, the strongest annual change rate was found in RD of the fornix crus ($t = 10.34$, $p < 0.0001$). These analyses indicate that neocortical Aβ deposition increased over time, whereas microstructural measures showed a pattern of decreased integrity. We conducted a series of multiple linear regression analyses examining the effects of baseline and age on annual change rate of each primary DTI index in both white matter ROIs, which is summarized in the Table 1 in Supplementary Materials. After FDR correction among the 6 tests (3 DTI indices × 2 ROIs), higher baseline FA was related to slower FA reduction in both the fornix crus ($p = 0.045$) and PHC-cingulum ($p = 0.006$), while the effect of baseline was not significant for RD or AXD in either ROI ($p > 0.10$).

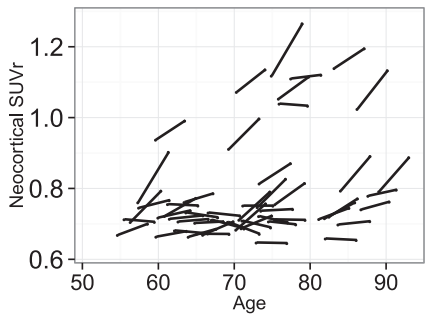

Fig. 2. Spaghetti plot of neocortical SUVr derived from Aβ-PET measured at baseline and follow-up. Abbreviations: Aβ, amyloid-beta; PET, positron emission tomography; SUVr, standard uptake value ratio.

3.3. Relationship of annual changes in cortical Aβ deposition and microstructures of the limbic tracts

We then assessed the primary hypothesis of the present study: do increases in neocortical Aβ burden predict microstructural changes in the fornix or PHC-cingulum? Fig. 1 in Supplementary Materials provides a qualitative look at individual measures of the 3 DTI indices in each ROI against overall neocortical Aβ burden at baseline and follow-up. To quantify the relationships of changes, we first used linear regression models to assess whether the annual change rate of neocortical SUVr predicted the annual change rate of each of the 3 DTI indices in the fornix crus and PHC-cingulum, for which age and gender were controlled. We found that an increase in neocortical SUVr predicted an increase in RD ($R^2 = 0.158$, $p = 0.003$) and AXD ($R^2 = 0.086$, $p = 0.034$) in the fornix crus, while there was no effect on the FA ($R^2 = 0.0007$, $p = 0.851$). There were no significant effects of annual changes in neocortical SUVr on annual changes in any DTI indices of the PHC-cingulum ($R^2 < 0.002$, $p > 0.80$). After FDR correction among the 6 tests (3 DTI indices × 2 ROIs), the effect of neocortical SUVr remained significant on RD ($p = 0.018$) but not AXD ($p = 0.170$) in the fornix crus. Fig. 3 displays the relationship between neocortical SUVr and RD in the fornix crus in both (Fig. 3A) the spaghetti plot of individual measures at baseline and follow-up and (Fig. 3B) the scatter plot of annual change rates. In a separate linear regression analysis of annual changes, we found no interaction of age by neocortical SUVr on RD in this ROI ($p = 0.69$).

We next examined whether this primary finding was affected by baseline neocortical Aβ load. It is of interest to examine whether microstructural changes in the white matter tracts may differ at different stages of preclinical AD. First, in a general linear regression model, we found that baseline neocortical SUVr was not significantly related to the annual change rate of RD of the fornix crus ($R^2 = 0.027$, $p = 0.24$), for which age and gender were controlled. Second, in the original linear regression model assessing the change-to-change relationship between neocortical SUVr and RD in the fornix crus, the primary finding remained significant after controlling for baseline neocortical SUVr as well as age and gender ($R^2 = 0.114$, $p = 0.01$). Third, we found no significant interaction of baseline by the annual change rate of neocortical SUVr ($p = 0.16$). These results indicate that the primary change-to-change relationship between neocortical Aβ load and the fornix was consistent regardless of the baseline status of neocortical Aβ load.

We also examined whether the primary finding was affected by baseline RD of the fornix crus. First, in a general linear regression model, baseline RD of the fornix crus was found not related to its annual change rate ($R^2 = 0.048$, $p = 0.12$), for which age and gender were controlled. Second, in the original linear regression model assessing the change-to-change relationship between neocortical SUVr and RD in the fornix crus, the primary finding remained significant after controlling for baseline RD of the fornix crus as well as age and gender ($R^2 = 0.110$, $p = 0.02$). There was also no interaction of baseline RD in the fornix crus and the annual change rate of neocortical SUVr ($p = 0.62$). These results indicate that the primary change-to-change relationship between neocortical Aβ load and the fornix was not dependent on the baseline microstructural measures of the fornix.

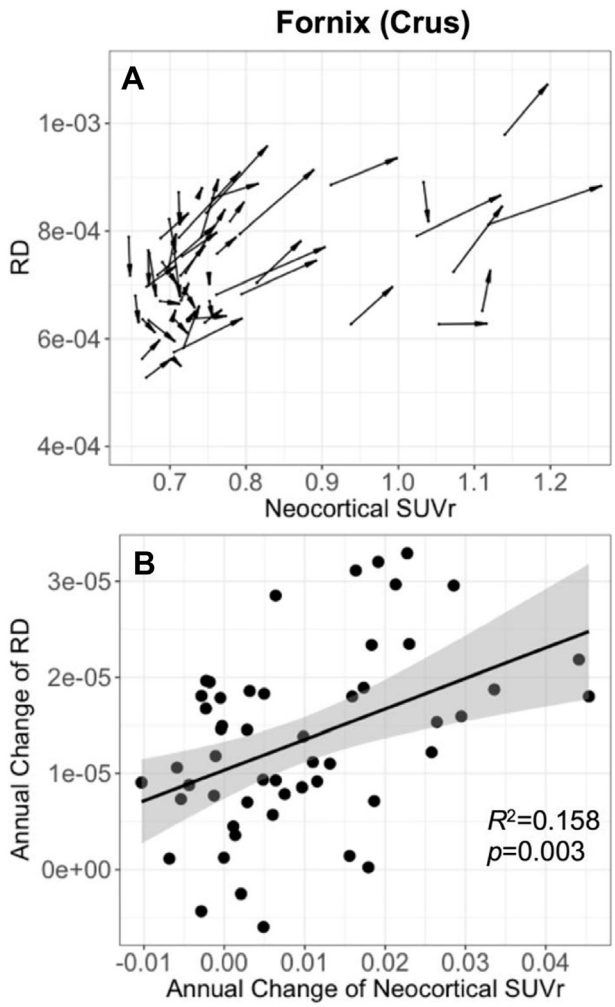

Fig. 3. (A) Spaghetti plots of the RD index in the ROI of the fornix crus against neocortical SUVr. The direction of each arrow points from baseline to follow-up in each individual participant. (B) Annual change rate of neocortical SUVr was associated with annual change rate of RD in the bilateral ROI of the fornix crus. The R^2 value was computed from linear regression analysis, for which age and gender were controlled. The gray shade area indicates 95% confidence interval of the regression. The diffusivity unit of RD is mm^2/s. Abbreviations: RD, radial diffusivity; ROI, region of interest; SUVr, standardized uptake value ratio.

In addition, we directly compared changes in the fornix and PHC-cingulum and their relationships to changes in neocortical Aβ burden. A paired *t*-test found that the annual increase rate of RD in the fornix crus was larger than that of the PHC-cingulum ($t = 7.012$, $p < 0.0001$). In a multiple linear regression analysis, we used the annual change rates of RD in both the fornix crus and PHC-cingulum to predict the annual change rate of neocortical SUVr, for which age and gender were controlled. We found that there was a main effect of annual change rate of RD in the fornix crus ($p = 0.003$) but not in the PHC-cingulum ($p = 0.52$).

We then conducted a series of secondary analyses to assess whether the primary finding (Fig. 3B) was influenced by additional covariates. The additional covariates included head motion during DTI acquisition (i.e., TMI), global brain atrophy (i.e., TCV normalized by intracranial volume), regional Aβ burden in the hippocampus (i.e., hippocampal SUVr), and summary DTI indices of the global white matter (i.e., MD and FA), all of which were measured at both baseline and follow-up. As summarized in Table 2, we assessed how much the relevant variance in the primary relationship would change after controlling for each additional covariate. In brief, the primary relationship remained significant in most of the modified models. Not surprisingly, the largest attenuation of the relevant variance was found in the modified model controlling for annual change rate of MD in the global white matter, where the primary relationship still approached to significance ($p = 0.058$).

3.4. Relationship of microstructure of the limbic tracts to episodic memory and other cognitive functions

Finally, we assessed whether white matter microstructure of the limbic tracts was related to episodic memory or other cognitive variables in cognitively normal adults, both cross-sectionally and longitudinally. It was expected that such a relationship might be weak, if present at all, in cognitively normal adults. To reduce the number of comparisons, we focused our analyses on RD of the fornix crus as shown in our primary finding.

We first assessed whether RD of the fornix crus predicted episodic memory or other cognitive outcomes at the baseline and follow-up, respectively. The relationship between RD of the fornix crus and episodic memory was not significant at either baseline ($R^2 < 0.001$, $p = 0.87$) or follow-up ($R^2 = 0.051$, $p = 0.12$), for which age and gender were controlled. Using the same approach, we also found that RD of the fornix crus was not significantly related to any of these cognitive variables at either the baseline or follow-up ($R^2 < 0.05$, $p > 0.10$), for which age and gender were controlled. We then examined the relationship of annual change in RD of the fornix crus and annual change in episodic memory or other cognitive variables. Annual change in RD of the fornix crus was not significantly related to annual change in episodic memory ($R^2 = 0.010$, $p = 0.50$) or other cognitive variables ($R^2 < 0.04$, $p > 0.20$), with age and gender controlled.

Overall, we found no evidence that RD of the fornix crus was related to episodic memory or other cognitive variables in this cognitively normal sample with either cross-sectional or longitudinal measures.

4. Discussion

In the present study, we report that an increase in neocortical Aβ burden predicted an increase in RD of the fornix crus over the same interval. There were no findings in any DTI indices of the PHC-cingulum. The relationship between neocortical Aβ and the fornix held after accounting for age, gender, and correction for multiple comparisons. Importantly, this relationship was not dependent on baseline measures of either neocortical Aβ burden or RD of the fornix crus. In a series of additional analyses of other covariates, we further confirmed that the primary finding held after accounting for head motion during DTI acquisition, global brain atrophy, global change in the white matter, and regional Aβ burden in the hippocampus. Finally, we found no evidence that increases in RD of the fornix contributed to declines in episodic memory or other cognitive outcomes in this cognitively normal sample, controlling for age and gender. This was not surprising in participants who were cognitively normal. We expect that the relationship between microstructure of the fornix and cognition would become more evident at a longer testing interval.

Our longitudinal data were consistent with several previous cross-sectional reports that higher neocortical Aβ burden is related to lower FA in the fornix of cognitively normal adults (Brown et al., 2017; Chao et al., 2013; Gold et al., 2014) because higher RD is often related to lower FA in white matter tracts. The relatively weak cross-sectional effect in our data, although approaching to significance, may demonstrate the advantage of using a longitudinal design to detect subtle brain changes in preclinical AD. In addition, the fact that the fornix crus ROI was only a limited portion of the

fornix might make it insensitive to microstructural changes in other parts of the fornix. This problem may be better addressed in future work with the use of a template of the entire fornix (Brown et al., 2017). Furthermore, the reason that we did not find an effect of neocortical Aβ burden on the FA index was likely due to greater sensitivity of RD compared to the ratio score that FA reflects (Acosta-Cabronero and Nestor, 2014; Nir et al., 2013). Higher RD in fiber tracts might reflect myelin loss in white matter tracts, together with possible changes in axonal density, axonal diameter, or fiber coherence, based on previous histological validation of DTI using human tissues (Concha, 2014).

We note that, with a larger sample, Rieckmann et al. reported an effect of baseline neocortical Aβ status on FA decreasing of the PHC-cingulum over about 2.5 years, while the fornix was not examined (Rieckmann et al., 2016). In contrast, we found no relationship between changes in neocortical Aβ burden and changes in the PHC-cingulum, a pattern that persisted across all of our analyses. Our data suggest that the fornix may be more vulnerable than the PHC-cingulum in the earliest phase of AD. Anatomical differences between the fornix and PHC-cingulum may explain their different vulnerability to preclinical AD. Specifically, the fornix directly connects to the hippocampus and contains both afferent and efferent fiber tracts (Kantarci, 2014; Mori and Aggarwal, 2014), whereas the PHC-cingulum contains predominantly afferent fibers to the MTL and does not directly connect to the hippocampus (Mori and Aggarwal, 2014; Mufson and Pandya, 1984). Further investigation is needed to clarify how connectivity and directionality of fiber tracts are relevant to their vulnerability (Braak and Del Tredici, 2011; Stopschinski and Diamond, 2017).

There are multiple pathological mechanisms that may link the Aβ pathology to microstructural changes in the fornix in preclinical AD. Because the fornix is a bidirectional fiber tract that connects many cortical and subcortical structures, either directly or indirectly, to the hippocampus (Aggleton, 2014; Catani et al., 2013), the development of Aβ pathology in the cortical regions may induce microstructural changes in the fornix. In addition, although the MTL structures have generally low susceptibility to neuritic Aβ plaques in preclinical AD (Arnold et al., 1991; Braak and Braak, 1991; Grothe et al., 2017), diffuse or soluble forms of Aβ may still develop in the MTL (Thal et al., 2000). Diffuse or soluble forms of Aβ may be more neurotoxic than plaques of Aβ (Mucke and Selkoe, 2012). There is evidence that diffuse or soluble forms of Aβ are cytotoxic to oligodendrocytes and may lead to white matter abnormality (Xu et al., 2001).

It is also possible that the MTL tau pathology may mediate the effect of neocortical Aβ burden on the fornix. The MTL is the earliest major brain region affected by deposition of tau tangles, which is a major hallmark of AD (Braak and Braak, 1991). There is mounting evidence in both postmortem and in vivo PET imaging studies in cognitively normal adults that neocortical Aβ deposition is a harbinger of the MTL tauopathy (Braak and Braak, 1991; Braak et al., 2011; Johnson et al., 2015; Lockhart et al., 2017; Scholl et al., 2016; Sepulcre et al., 2016). The tauopathy may lead to neural dysfunction and neurodegeneration in the local brain network (Hoover et al., 2010; Menkes-Caspi et al., 2015; Spires et al., 2006). Particularly, the MTL tau pathology has been associated with fiber degradation in the fornix and PHC-cingulum, in both postmortem histology (Hopper and Vogel, 1976) and in vivo DTI studies of AD patients (Kantarci, 2014; Nir et al., 2013; Oishi and Lyketsos, 2014). The tau pathology may also interact with soluble or diffuse Aβ, particularly in the MTL, and induce more detrimental effects on both neurons and neural fibers (Bloom, 2014; Palop and Mucke, 2016; Shukla and Bridges, 2001).

It is also recognized that myelin loss in white matter fiber tracts may be induced by other age-related pathological factors independent of Aβ or tau (Bartzokis, 2004). Demyelination of the white matter has been reported to occur before the presence of Aβ plaques and tau tangles in preclinical AD (Sachdev et al., 2013). It is further theorized that white matter degradation may possibly serve as an independent pathological pathway that may induce AD-related Aβ and tau pathologies (Bartzokis, 2004). Further work is needed to clarify the mechanistic relationship between white matter degradation and other AD-related pathologies.

4.1. Methodological issues

There are several methodological issues of the present DTI method that deserve consideration. First, the single tensor model of water diffusion in DTI relies on the assumption that there is a single, coherent fiber population in each voxel (Jones et al., 2012). Although both the fornix and PHC-cingulum do not normally cross with other major white matter fibers, fiber arrangement may become less coherent under the influence of pathology. Second, the behavior of water diffusion relies on cellular components adjacent to axonal fibers such as glial cells, vascular capillary bed, and extracellular spaces, which may also change with a variety of age-related pathologies. Third, both the fornix and PHC-cingulum are relatively small fiber tracts in the brain. In addition, the ROIs in the JHU template were only portions of the structures (Mori et al., 2008). It is technically challenging to align small ROIs precisely across individuals. We addressed this issue by using a state-of-art image registration method ANTS (Avants et al., 2014) and by creating a sample-specific FA template. Future studies may benefit from some recent developments of anatomical templates of these fiber structures (Brown et al., 2017).

Fourth, because both the fornix and PHC-cingulum are adjacent to the ventricles and brain atrophy is commonly presented in the brain of older adults, partial volume effects of CSF near these fiber tracts may result in imaging artifacts in DTI (Concha et al., 2005). The partial volume effect may be more severe in participants due to brain atrophy (Metzler-Baddeley et al., 2012), which may introduce bias in the statistical analyses. Methods of free-water elimination are proposed to address the problem of partial volume effects (Pasternak et al., 2009), but it is an ill-posed problem with a single b-value in conventional DTI (Hoy et al., 2014). An accurate estimation of free-water elimination requires at least 2 b-value acquisitions (Hoy et al., 2014), or other advanced diffusion models (Assaf and Basser, 2005; Zhang et al., 2012). We partially addressed the problem of CSF contamination and partial volume effects in DTI. First, we excluded voxels from each anatomical ROI where the FA value was lower than 0.2 in the FA template. This was to ensure that our measurements were located in voxels composed mainly of the white matter. Second, we took global brain atrophy into account in the secondary analyses and found the primary finding remained significant, although attenuated, after controlling for normalized TCV (Table 2). It was also confirmed that the effect of neocortical Aβ burden was found only on RD but not AXD in the fornix ROI. If DTI signal was contaminated by CSF because of brain atrophy, it would be more likely that a relationship would be detected between Aβ and both RD and AXD in the fornix.

5. Conclusions

In the present study of cognitively normal adults, we found that an increase in neocortical Aβ burden was associated with an increase of RD in the fornix, for which age and gender were controlled. This relationship was not dependent on baseline measures of either neocortical Aβ burden or RD of the fornix crus. In contrast, there were no significant effects of changes in neocortical Aβ burden on changes in the PHC-cingulum. In addition, we found

no significant cross-sectional relationship between neocortical Aβ burden and DTI indices in the fornix at baseline. These data demonstrate the advantage of using a longitudinal design to detect subtle brain changes in preclinical AD. In addition, microstructural changes in the fornix were not yet related to decline of episodic memory or other cognitive outcomes. Overall our data suggest an early sign of white matter degradation in the core memory network in preclinical AD.

Disclosure statement

The authors have no actual or potential conflicts of interest.

Acknowledgements

This research was supported by the National Institutes of Health (Grant 5R37AG006265 to DCP) and Avid Radiopharmaceuticals, a division of Eli Lilly, who provided Florbetapir PET tracers and some support for personnel. The authors thank Dr. Melissa Rundle for coordinating the project and Andrew Hebrank for assistance in image processing.

Appendix A. Supplementary data

Supplementary data associated with this article can be found, in the online version, at https://doi.org/10.1016/j.neurobiolaging.2018.02.021.

References

Acosta-Cabronero, J., Nestor, P.J., 2014. Diffusion tensor imaging in Alzheimer's disease: insights into the limbic-diencephalic network and methodological considerations. Front. Aging Neurosci. 6, 266.

Aggleton, J.P., 2014. Looking beyond the hippocampus: old and new neurological targets for understanding memory disorders. Proc. Biol. Sci. 281. https://doi.org/10.1098/rspb.2014.0565.

Arnold, S.E., Hyman, B.T., Flory, J., Damasio, A.R., Van Hoesen, G.W., 1991. The topographical and neuroanatomical distribution of neurofibrillary tangles and neuritic plaques in the cerebral cortex of patients with Alzheimer's disease. Cereb. Cortex 1, 103–116.

Assaf, Y., Basser, P.J., 2005. Composite hindered and restricted model of diffusion (CHARMED) MR imaging of the human brain. NeuroImage 27, 48–58.

Avants, B., Gee, J.C., 2004. Geodesic estimation for large deformation anatomical shape averaging and interpolation. NeuroImage 23 (Suppl 1), S139–S150.

Avants, B.B., Tustison, N.J., Stauffer, M., Song, G., Wu, B., Gee, J.C., 2014. The Insight ToolKit image registration framework. Front. Neuroinform. 8, 44.

Bartzokis, G., 2004. Age-related myelin breakdown: a developmental model of cognitive decline and Alzheimer's disease. Neurobiol. Aging 25, 5–18 author reply 49–62.

Basser, P.J., Pierpaoli, C., 1996. Microstructural and physiological features of tissues elucidated by quantitative-diffusion-tensor MRI. J. Magn. Reson. Ser. B 111, 209–219.

Bloom, G.S., 2014. Amyloid-beta and tau: the trigger and bullet in Alzheimer disease pathogenesis. JAMA Neurol. 71, 505–508.

Braak, H., Braak, E., 1991. Neuropathological stageing of Alzheimer-related changes. Acta Neuropathol. 82, 239–259.

Braak, H., Del Tredici, K., 2011. Alzheimer's pathogenesis: is there neuron-to-neuron propagation? Acta Neuropathol. 121, 589–595.

Braak, H., Thal, D.R., Ghebremedhin, E., Del Tredici, K., 2011. Stages of the pathologic process in Alzheimer disease: age categories from 1 to 100 years. J. Neuropathol. Exp. Neurol. 70, 960–969.

Brandt, J., 1991. The Hopkins verbal learning test: development of a new memory test with six equivalent forms. Clin. Neuropsychol. 5, 125–142.

Brown, C.A., Johnson, N.F., Anderson-Mooney, A.J., Jicha, G.A., Shaw, L.M., Trojanowski, J.Q., Van Eldik, L.J., Schmitt, F.A., Smith, C.D., Gold, B.T., 2017. Development, validation and application of a new fornix template for studies of aging and preclinical Alzheimer's disease. NeuroImage Clin. 13, 106–115.

Catani, M., Dell'acqua, F., Thiebaut de Schotten, M., 2013. A revised limbic system model for memory, emotion and behaviour. Neurosci. Biobehav. Rev. 37, 1724–1737.

Chao, L.L., Decarli, C., Kriger, S., Truran, D., Zhang, Y., Laxamana, J., Villeneuve, S., Jagust, W.J., Sanossian, N., Mack, W.J., Chui, H.C., Weiner, M.W., 2013. Associations between white matter hyperintensities and beta amyloid on integrity of projection, association, and limbic fiber tracts measured with diffusion tensor MRI. PLoS One 8, e65175.

Concha, L., 2014. A macroscopic view of microstructure: using diffusion-weighted images to infer damage, repair, and plasticity of white matter. Neuroscience 276, 14–28.

Concha, L., Gross, D.W., Beaulieu, C., 2005. Diffusion tensor tractography of the limbic system. AJNR Am. J. Neuroradiol. 26, 2267–2274.

Ekstrom, R.B., French, J.W., Harman, H., Derman, D., 1976. Kit of Factor-referenced Cognitive Tests (rev. ed.). Educational Testing Service, Princeton, NJ.

Farrell, M.E., Kennedy, K.M., Rodrigue, K.M., Wig, G., Bischof, G.N., Rieck, J.R., Chen, X., Festini, S.B., Devous Sr., M.D., Park, D.C., 2017. Association of longitudinal cognitive decline with amyloid burden in middle-aged and older adults: evidence for a dose-response relationship. JAMA Neurol. 74, 830–838.

Gallagher, M., Koh, M.T., 2011. Episodic memory on the path to Alzheimer's disease. Curr. Opin. Neurobiol. 21, 929–934.

Gold, B.T., Zhu, Z., Brown, C.A., Andersen, A.H., LaDu, M.J., Tai, L., Jicha, G.A., Kryscio, R.J., Estus, S., Nelson, P.T., Scheff, S.W., Abner, E., Schmitt, F.A., Van Eldik, L.J., Smith, C.D., 2014. White matter integrity is associated with cerebrospinal fluid markers of Alzheimer's disease in normal adults. Neurobiol. Aging 35, 2263–2271.

Grothe, M.J., Barthel, H., Sepulcre, J., Dyrba, M., Sabri, O., Teipel, S.J. Alzheimer's Disease Neuroimaging, I., 2017. In vivo staging of regional amyloid deposition. Neurology 89, 2031–2038.

Hardy, J., Selkoe, D.J., 2002. The amyloid hypothesis of Alzheimer's disease: progress and problems on the road to therapeutics. Science 297, 353–356.

Hoover, B.R., Reed, M.N., Su, J., Penrod, R.D., Kotilinek, L.A., Grant, M.K., Pitstick, R., Carlson, G.A., Lanier, L.M., Yuan, L.L., Ashe, K.H., Liao, D., 2010. Tau mislocalization to dendritic spines mediates synaptic dysfunction independently of neurodegeneration. Neuron 68, 1067–1081.

Hopper, M.W., Vogel, F.S., 1976. The limbic system in Alzheimer's disease. A neuropathologic investigation. Am. J. Pathol. 85, 1–20.

Hoy, A.R., Koay, C.G., Kecskemeti, S.R., Alexander, A.L., 2014. Optimization of a free water elimination two-compartment model for diffusion tensor imaging. NeuroImage 103, 323–333.

Ittner, L.M., Gotz, J., 2011. Amyloid-beta and tau–a toxic pas de deux in Alzheimer's disease. Nat. Rev. Neurosci. 12, 65–72.

Jack Jr., C.R., Holtzman, D.M., 2013. Biomarker modeling of Alzheimer's disease. Neuron 80, 1347–1358.

Jack Jr., C.R., Knopman, D.S., Jagust, W.J., Shaw, L.M., Aisen, P.S., Weiner, M.W., Petersen, R.C., Trojanowski, J.Q., 2010. Hypothetical model of dynamic biomarkers of the Alzheimer's pathological cascade. Lancet Neurol. 9, 119–128.

Jack Jr., C.R., Petersen, R.C., Xu, Y.C., Waring, S.C., O'Brien, P.C., Tangalos, E.G., Smith, G.E., Ivnik, R.J., Kokmen, E., 1997. Medial temporal atrophy on MRI in normal aging and very mild Alzheimer's disease. Neurology 49, 786–794.

Jenkinson, M., Beckmann, C.F., Behrens, T.E., Woolrich, M.W., Smith, S.M., 2012. FSL. NeuroImage 62, 782–790.

Jin, M., Shepardson, N., Yang, T., Chen, G., Walsh, D., Selkoe, D.J., 2011. Soluble amyloid beta-protein dimers isolated from Alzheimer cortex directly induce Tau hyperphosphorylation and neuritic degeneration. Proc. Natl. Acad. Sci. U. S. A. 108, 5819–5824.

Johnson, K.A., Schultz, A., Betensky, R.A., Becker, J.A., Sepulcre, J., Rentz, D., Mormino, E., Chhatwal, J., Amariglio, R., Papp, K., Marshall, G., Albers, M., Mauro, S., Pepin, L., Alverio, J., Judge, K., Philiossaint, M., Shoup, T., Yokell, D., Dickerson, B., Gomez-Isla, T., Hyman, B., Vasdev, N., Sperling, R., 2015. Tau PET imaging in aging and early Alzheimer's disease. Ann. Neurol. 79, 110–119.

Jones, D.K., Knosche, T.R., Turner, R., 2012. White matter integrity, fiber count, and other fallacies: the do's and don'ts of diffusion MRI. NeuroImage 73, 239–254.

Kanaan, N.M., Pigino, G.F., Brady, S.T., Lazarov, O., Binder, L.I., Morfini, G.A., 2013. Axonal degeneration in Alzheimer's disease: when signaling abnormalities meet the axonal transport system. Exp. Neurol. 246, 44–53.

Kantarci, K., 2014. Fractional anisotropy of the fornix and hippocampal atrophy in Alzheimer's disease. Front. Aging Neurosci. 6, 316.

Kantarci, K., Murray, M.E., Schwarz, C.G., Reid, R.I., Przybelski, S.A., Lesnick, T., Zuk, S.M., Raman, M.R., Senjem, M.L., Gunter, J.L., Boeve, B.F., Knopman, D.S., Parisi, J.E., Petersen, R.C., Jack Jr., C.R., Dickson, D.W., 2017. White-matter integrity on DTI and the pathologic staging of Alzheimer's disease. Neurobiol. Aging 56, 172–179.

Landau, S.M., Fero, A., Baker, S.L., Koeppe, R., Mintun, M., Chen, K., Reiman, E.M., Jagust, W.J., 2015. Measurement of longitudinal beta-amyloid change with 18F-florbetapir PET and standardized uptake value ratios. J. Nucl. Med. 56, 567–574.

Lockhart, S.N., Scholl, M., Baker, S.L., Ayakta, N., Swinnerton, K.N., Bell, R.K., Mellinger, T.J., Shah, V.D., O'Neil, J.P., Janabi, M., Jagust, W.J., 2017. Amyloid and tau PET demonstrate region-specific associations in normal older people. NeuroImage 150, 191–199.

Madden, D.J., Bennett, I.J., Burzynska, A., Potter, G.G., Chen, N.K., Song, A.W., 2012. Diffusion tensor imaging of cerebral white matter integrity in cognitive aging. Biochim. Biophys. Acta 1822, 386–400.

Malykhin, N., Concha, L., Seres, P., Beaulieu, C., Coupland, N.J., 2008. Diffusion tensor imaging tractography and reliability analysis for limbic and paralimbic white matter tracts. Psychiatry Res. 164, 132–142.

Menkes-Caspi, N., Yamin, H.G., Kellner, V., Spires-Jones, T.L., Cohen, D., Stern, E.A., 2015. Pathological tau disrupts ongoing network activity. Neuron 85, 959–966.

Metzler-Baddeley, C., O'Sullivan, M.J., Bells, S., Pasternak, O., Jones, D.K., 2012. How and how not to correct for CSF-contamination in diffusion MRI. NeuroImage 59, 1394–1403.

Mori, S., Aggarwal, M., 2014. In vivo magnetic resonance imaging of the human limbic white matter. Front. Aging Neurosci. 6, 321.

Mori, S., Oishi, K., Jiang, H., Jiang, L., Li, X., Akhter, K., Hua, K., Faria, A.V., Mahmood, A., Woods, R., Toga, A.W., Pike, G.B., Neto, P.R., Evans, A., Zhang, J., Huang, H., Miller, M.I., van Zijl, P., Mazziotta, J., 2008. Stereotaxic white matter atlas based on diffusion tensor imaging in an ICBM template. NeuroImage 40, 570–582.

Mormino, E.C., Brandel, M.G., Madison, C.M., Rabinovici, G.D., Marks, S., Baker, S.L., Jagust, W.J., 2012. Not quite PIB-positive, not quite PIB-negative: slight PIB elevations in elderly normal control subjects are biologically relevant. NeuroImage 59, 1152–1160.

Mucke, L., Selkoe, D.J., 2012. Neurotoxicity of amyloid beta-protein: synaptic and network dysfunction. Cold Spring Harbor Perspect. Med. 2, a006338.

Mufson, E.J., Pandya, D.N., 1984. Some observations on the course and composition of the cingulum bundle in the rhesus monkey. J. Comp. Neurol. 225, 31–43.

Nir, T.M., Jahanshad, N., Villalon-Reina, J.E., Toga, A.W., Jack, C.R., Weiner, M.W., Thompson, P.M. Alzheimer's Disease Neuroimaging, I., 2013. Effectiveness of regional DTI measures in distinguishing Alzheimer's disease, MCI, and normal aging. NeuroImage Clin. 3, 180–195.

Oishi, K., Lyketsos, C.G., 2014. Alzheimer's disease and the fornix. Front. Aging Neurosci. 6, 241.

Palop, J.J., Mucke, L., 2016. Network abnormalities and interneuron dysfunction in Alzheimer disease. Nat. Rev. Neurosci. 17, 777–792.

Pasternak, O., Sochen, N., Gur, Y., Intrator, N., Assaf, Y., 2009. Free water elimination and mapping from diffusion MRI. Magn. Reson. Med. 62, 717–730.

Petersen, R.C., Jack Jr., C.R., Xu, Y.C., Waring, S.C., O'Brien, P.C., Smith, G.E., Ivnik, R.J., Tangalos, E.G., Boeve, B.F., Kokmen, E., 2000. Memory and MRI-based hippocampal volumes in aging and AD. Neurology 54, 581–587.

Racine, A.M., Adluru, N., Alexander, A.L., Christian, B.T., Okonkwo, O.C., Oh, J., Cleary, C.A., Birdsill, A., Hillmer, A.T., Murali, D., Barnhart, T.E., Gallagher, C.L., Carlsson, C.M., Rowley, H.A., Dowling, N.M., Asthana, S., Sager, M.A., Bendlin, B.B., Johnson, S.C., 2014. Associations between white matter microstructure and amyloid burden in preclinical Alzheimer's disease: a multimodal imaging investigation. NeuroImage Clin. 4, 604–614.

Raven, J., Raven, J.C., Court, J.H., 1998. Manual for Raven's Progressive Matrices and Vocabulary Scale. The Psychological Corporation, San Antonio, TX.

Rieckmann, A., Van Dijk, K.R., Sperling, R.A., Johnson, K.A., Buckner, R.L., Hedden, T., 2016. Accelerated decline in white matter integrity in clinically normal individuals at risk for Alzheimer's disease. Neurobiol. Aging 42, 177–188.

Ringman, J.M., O'Neill, J., Geschwind, D., Medina, L., Apostolova, L.G., Rodriguez, Y., Schaffer, B., Varpetian, A., Tseng, B., Ortiz, F., Fitten, J., Cummings, J.L., Bartzokis, G., 2007. Diffusion tensor imaging in preclinical and presymptomatic carriers of familial Alzheimer's disease mutations. Brain 130, 1767–1776.

Robbins, T.W., James, M., Owen, A.M., Sahakian, B.J., McInnes, L., Rabbitt, P., 1994. Cambridge Neuropsychological Test Automated Battery (CANTAB): a factor analytic study of a large sample of normal elderly volunteers. Dementia 5, 266–281.

Sachdev, P.S., Zhuang, L., Braidy, N., Wen, W., 2013. Is Alzheimer's a disease of the white matter? Curr. Opin. Psychiatry 26, 244–251.

Salthouse, T.A., Babcock, R.L., 1991. Decomposing adult age differences in working memory. Dev. Psychol. 27, 763–776.

Sanchez-Valle, R., Monte, G.C., Sala-Llonch, R., Bosch, B., Fortea, J., Llado, A., Antonell, A., Balasa, M., Bargallo, N., Molinuevo, J.L., 2016. White matter abnormalities track disease progression in PSEN1 autosomal dominant Alzheimer's disease. J. Alzheimer's Dis. 51, 827–835.

Scholl, M., Lockhart, S.N., Schonhaut, D.R., O'Neil, J.P., Janabi, M., Ossenkoppele, R., Baker, S.L., Vogel, J.W., Faria, J., Schwimmer, H.D., Rabinovici, G.D., Jagust, W.J., 2016. PET imaging of tau deposition in the aging human brain. Neuron 89, 971–982.

Schwarz, C.G., Reid, R.I., Gunter, J.L., Senjem, M.L., Przybelski, S.A., Zuk, S.M., Whitwell, J.L., Vemuri, P., Josephs, K.A., Kantarci, K., Thompson, P.M., Petersen, R.C., Jack Jr., C.R., 2014. Improved DTI registration allows voxel-based analysis that outperforms Tract-Based Spatial Statistics. NeuroImage 94, 65–78.

Schwarz, C.G., Senjem, M.L., Gunter, J.L., Tosakulwong, N., Weigand, S.D., Kemp, B.J., Spychalla, A.J., Vemuri, P., Petersen, R.C., Lowe, V.J., Jack Jr., C.R., 2017. Optimizing PiB-PET SUVR change-over-time measurement by a large-scale analysis of longitudinal reliability, plausibility, separability, and correlation with MMSE. NeuroImage 144, 113–127.

Selkoe, D.J., 2002. Alzheimer's disease is a synaptic failure. Science 298, 789–791.

Sepulcre, J., Schultz, A.P., Sabuncu, M., Gomez-Isla, T., Chhatwal, J., Becker, A., Sperling, R., Johnson, K.A., 2016. In vivo tau, amyloid, and gray matter profiles in the aging brain. J. Neurosci. 36, 7364–7374.

Shukla, C., Bridges, L.R., 2001. Tau, beta-amyloid and beta-amyloid precursor protein distribution in the entorhinal-hippocampal alvear and perforant pathways in the Alzheimer's brain. Neurosci. Lett. 303, 193–197.

Small, S.A., Schobel, S.A., Buxton, R.B., Witter, M.P., Barnes, C.A., 2011. A pathophysiological framework of hippocampal dysfunction in ageing and disease. Nat. Rev. Neurosci. 12, 585–601.

Solodkin, A., Chen, E.E., Van Hoesen, G.W., Heimer, L., Shereen, A., Kruggel, F., Mastrianni, J., 2013. In vivo parahippocampal white matter pathology as a biomarker of disease progression to Alzheimer's disease. J. Comp. Neurol. 521, 4300–4317.

Sperling, R.A., Aisen, P.S., Beckett, L.A., Bennett, D.A., Craft, S., Fagan, A.M., Iwatsubo, T., Jack Jr., C.R., Kaye, J., Montine, T.J., Park, D.C., Reiman, E.M., Rowe, C.C., Siemers, E., Stern, Y., Yaffe, K., Carrillo, M.C., Thies, B., Morrison-Bogorad, M., Wagster, M.V., Phelps, C.H., 2011. Toward defining the preclinical stages of Alzheimer's disease: recommendations from the National Institute on Aging-Alzheimer's Association workgroups on diagnostic guidelines for Alzheimer's disease. J. Alzheimer's Assoc. 7, 280–292.

Sperling, R.A., Dickerson, B.C., Pihlajamaki, M., Vannini, P., LaViolette, P.S., Vitolo, O.V., Hedden, T., Becker, J.A., Rentz, D.M., Selkoe, D.J., Johnson, K.A., 2010. Functional alterations in memory networks in early Alzheimer's disease. Neuromol. Med. 12, 27–43.

Spires, T.L., Orne, J.D., SantaCruz, K., Pitstick, R., Carlson, G.A., Ashe, K.H., Hyman, B.T., 2006. Region-specific dissociation of neuronal loss and neurofibrillary pathology in a mouse model of tauopathy. Am. J. Pathol. 168, 1598–1607.

Stopschinski, B.E., Diamond, M.I., 2017. The prion model for progression and diversity of neurodegenerative diseases. Lancet Neurol. 16, 323–332.

Thal, D.R., Rub, U., Schultz, C., Sassin, I., Ghebremedhin, E., Del Tredici, K., Braak, E., Braak, H., 2000. Sequence of Abeta-protein deposition in the human medial temporal lobe. J. Neuropathol. Exp. Neurol. 59, 733–748.

Villeneuve, S., Rabinovici, G.D., Cohn-Sheehy, B.I., Madison, C., Ayakta, N., Ghosh, P.M., La Joie, R., Arthur-Bentil, S.K., Vogel, J.W., Marks, S.M., Lehmann, M., Rosen, H.J., Reed, B., Olichney, J., Boxer, A.L., Miller, B.L., Borys, E., Jin, L.W., Huang, E.J., Grinberg, L.T., DeCarli, C., Seeley, W.W., Jagust, W., 2015. Existing Pittsburgh Compound-B positron emission tomography thresholds are too high: statistical and pathological evaluation. Brain 138, 2020–2033.

Wechsler, D., 1997. Wechsler Adult Intelligence Scale–iii (WAIS-iii). Psychological Corporation, New York.

Xu, J., Chen, S., Ahmed, S.H., Chen, H., Ku, G., Goldberg, M.P., Hsu, C.Y., 2001. Amyloid-beta peptides are cytotoxic to oligodendrocytes. J. Neurosci. 21, RC118.

Yendiki, A., Koldewyn, K., Kakunoori, S., Kanwisher, N., Fischl, B., 2013. Spurious group differences due to head motion in a diffusion MRI study. NeuroImage 88C, 79–90.

Zhang, H., Schneider, T., Wheeler-Kingshott, C.A., Alexander, D.C., 2012. NODDI: practical in vivo neurite orientation dispersion and density imaging of the human brain. NeuroImage 61, 1000–1016.